BURNER RIG HOT CORROSION OF A SINGLE CRYSTAL Ni-48Al-Ti-Hf-Ga ALLOY

J.A. NESBITT, R. DAROLIA* and M.D. CUY**
NASA Lewis Research Center, Cleveland, OH 44135
* General Electric Aircraft Engines (GEAE), Cincinnati, OH 45215
** Dynacs, Lewis Research Center Group, Cleveland, OH 44135

ABSTRACT

The hot corrosion resistance of a single crystal Ni-48Al-1Ti-0.5Hf-0.2Ga‡ alloy was examined in a Mach 0.3 burner rig at 900°C for 300 hours. The combustion chamber was doped with 2 ppmw synthetic sea salt. The hot corrosion attack produced a random mound morphology on the surface. Microstructurally, the hot corrosion attack appeared to initiate with oxide-filled pits which were often broad and shallow. At an intermediate stage, the pits increased in size to incorporate unoxidized Ni islands in the corrosion product. The rampant attack stage, which was observed only at sharp sample corners, was characterized by rapid inward growth of alumina in finger-like protrusions incorporating significant amounts of Al-depleted Ni islands. Aluminum consumption in the oxide fingers resulted in the growth of a γ' layer ahead of the advancing oxide fingers.

INTRODUCTION

Single-crystal nickel aluminide has undergone considerable investigation this decade as a potential structural material in aero gas turbine engines. The attractive features of NiAl in comparison to Ni-base superalloys include a higher melting point, lower density, higher thermal conductivity and excellent oxidation resistance [1]. However, binary NiAl suffers from a lack of ductility and fracture toughness at low temperatures, and low creep strength at high temperatures. These physical and mechanical properties have recently been reviewed in detail elsewhere [2]. Alloying additions of Hf, Ga, Ti and Cr have each shown some benefit to the mechanical properties over that of the binary alloy [3]. However, the collective effect of these alloying additions on the environmental resistance of NiAl was unclear. Hence, the purpose of the present study was to examine the hot corrosion behavior of a baseline alloy containing small amounts of Hf, Ga, and Ti.

Extensive work has been performed to understand the hot corrosion attack of superalloys and coatings and numerous review papers have been written [4,5]. In comparison, much less work as been performed on NiAl or NiAl-X alloys. Early studies found β-NiAl relatively resistant to Na_2SO_4 attack although the lower-Al, γ' Ni_3Al phase was not [6-9]. Kaufman concluded that "major attack on NiAl is preceded by transformation of a surface layer to Ni_3Al due to Al loss to the otherwise protective Al_2O_3 scale" [6]. Although Kaufman also reported that

‡ All concentrations are given in atomic percent.

additions of 10%Ti to β NiAl improved the hot corrosion resistance, McCarron, et al., reported that Ti additions definitely degraded the corrosion resistance of γ' Ni_3Al [8].

EXPERIMENTAL PROCEDURE

Single-crystal Ni-50Al-0.5Hf-0.1Ga-1.0Ti material was supplied by General Electric Aircraft Engines (GEAE). The material had been homogenized for 32 hrs at 1371°C (2500°F), HIP'ped for 6 hrs at 1371°C (2500°F) and 138 Mpa (20 Ksi), aged for 30 min at 1371°C (2500°F), cooled to 982°C (1800F) at 55°C/min (100°F/min), and finally held for 6 hrs at 982°C (1800°F) before cooling to room temperature. This processing produced a microstructure containing small oxide, carbide and Hf-containing intermetallic precipitates [10]. The carbides were identified as either HfC or (Hf,Ti)C and the oxide was identified as HfO_2. The oxides and carbides were often agglomerated. The intermetallic precipitates were relatively large (~1 μm) and were likely the Heusler Ni_2AlHf phase.

Samples were machined into hollow right circular cylinders with approximate dimensions of 1.27cm (0.5 in) outer diameter, 0.635cm (0.25 in) inner diameter by 1.27cm (0.5 in) height. All machining was accomplished by wire EDM. Due to limited material, samples were cut from single-crystal bars without regard to crystal orientation. All samples underwent a chemical milling treatment for 30 minutes at GEAE in order to remove the EDM recast layer.

The samples were tested in a Mach 0.3 burner rig at the Lewis Research Center. Jet A fuel was burned and a synthetic sea salt solution was injected into the burner to yield a concentration of 2 ppmw in the hot combustor exhaust. The samples and individual holders were fixtured on a twelve position carousel which rotated at 250-300 RPM in the flame of the burner. The samples underwent testing for 300 1-hr cycles. After each 1-hr exposure, the burner was shifted away exposing the samples to a high velocity, ambient temperature air stream to cool the samples for a minimum of 6 minutes. The fuel to air ratio in the burner was maintained at approximately 0.062 to yield average sample temperatures of 900±15°C (1652°F) as monitored using both a two-color and a laser pyrometer aimed at the rotating samples. Further details of the testing are given elsewhere [11].

RESULTS AND DISCUSSION

After 300 hrs of testing, a number of corrosion mounds were present on the ends and curved surface of the sample (Fig 1). Increased attack at the ID and OD edges resulted in the formation of a corrosion product "lip". X-ray diffraction of the ends and curved surface indicated the presence of α-Al_2O_3, NiO, a spinel phase (a_o=8.30A), TiO_2 and HfO_2. The β-NiAl substrate peak was also observed.

A cross-sectional SEM micrograph of the smooth oxide scale away from any corrosion mounds after 300 cycles of testing is shown in Fig 2a. The scale has a distinct inner and outer region with the inner region containing bright particles. EDS spectra (Fig 2b,c) reveal that both regions are Al rich, i.e., Al_2O_3. The outer region contains significant amounts of Ca and Mg from the sea salt, although Na, the major constituent of the salt, was not detected. The Fe and Cr detected in the outer region were commonly observed and result from deposition of Fe, Ni, Cr, Si and Mn from the corrosion of the burner and nozzle. Ti and Hf were also detected in both regions but at higher levels in the inner region. The bright particles within the inner region are

Hf-rich and presumably HfO_2. The bright particles in the alloy below the oxide scale are also HfO_2 which is preferentially oxidized before the Al and Ti. Although the O solubility in NiAl should be extremely small, some O diffuses into the alloy and internally oxidizes the oxygen-active Hf.

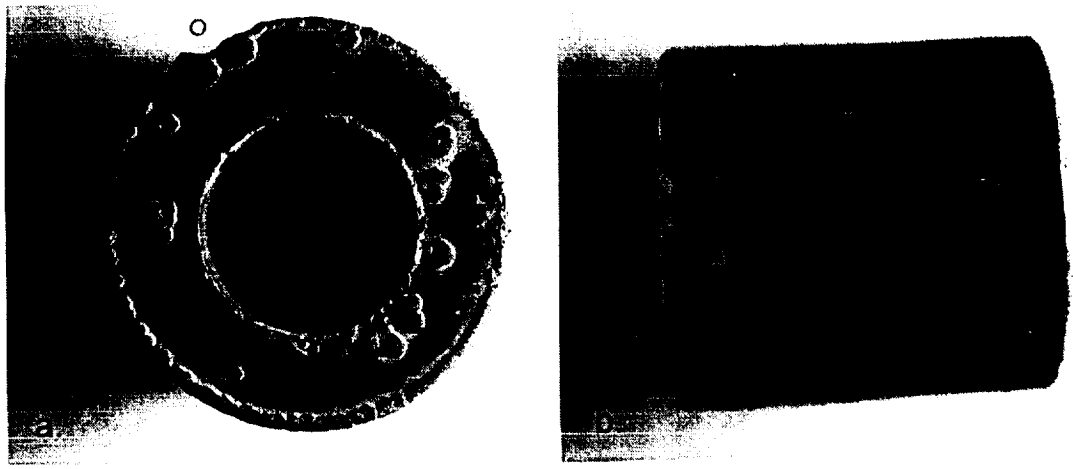

Figure 1. Macrophotos of one end and the curved surface after 300 hrs of testing.

The HfO_2 particles in the uniform scale (Fig 2a) serve as markers to indicate that for some period of time, the Al_2O_3 scale was growing outward. Since α-Al_2O_3 grows inward, it is very likely that during an early portion of the test, θ-Al_2O_3 formed and grew on the surface. θ-Al_2O_3, a metastable phase, commonly forms during oxidation of NiAl at temperatures below 1000°C and can remain on the surface for extended periods. θ-Al_2O_3 is also known to grow rapidly outward at a rate nearly two orders of magnitude faster than α-Al_2O_3 [12,13]. At higher temperatures (i.e., >1100°C), θ-Al_2O_3 typically transforms rapidly to α-Al_2O_3 although this

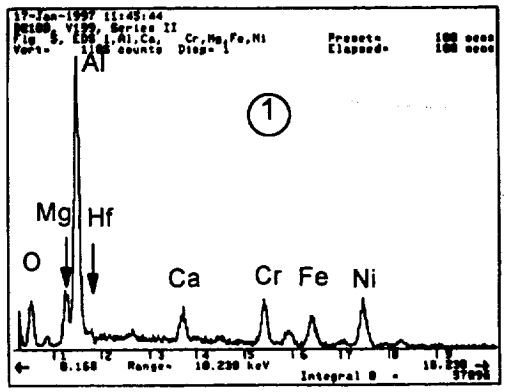

b.

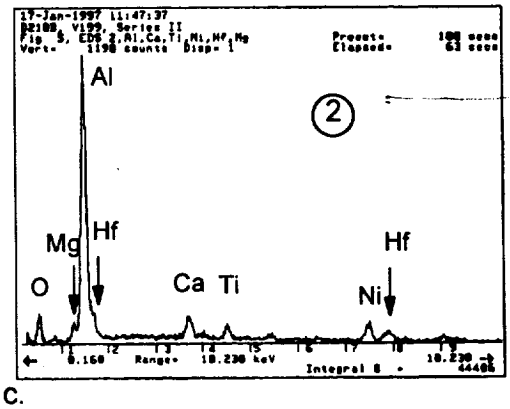

c.

Figure 2. SEM cross-sectional microstructure of smooth scale. EDS of the outer region of the scale is shown in b, and of the inner region in c. Bright particles in inner region and in alloy are probably HfO_2.

transformation is also affected by various elements in the alloy [12,13]. Since no θ-Al_2O_3 was detected by x-ray diffraction in the current study, any θ-Al_2O_3 could have transformed to α-Al_2O_3 prior to the first x-ray diffraction measurements made after 50 hrs. Elements within the alloy or deposited on the surface from the burner could also have aided the transformation at 900°C.

Certain oxide morphologies suggest the microstructural evolution leading to corrosion mound initiation. Figure 3a and b show two possible initiation morphologies, the former with a small "bulb" type pit and the latter with a much broader, shallow pit. The EDS spectra taken within the "bulb" pit (Fig 3c) indicates Al, Ca and Ti, the same elements as in the smooth region of scale (Fig 2b,c). EDS spectra of broad, shallow pits showed similar spectra although some contained little or no detectable Ca. Bright Hf-rich particles were present below most pits.

Concentration measurements made by electron microprobe in and below the broad, shallow pit are shown in Fig 3d. The Al gradient in the alloy indicates Al diffusion to the pit, whereas, the Ti gradient indicates some transport of Ti away from the pit. However, it is apparent that the Ti concentration in the pit is nearly equal to that in the alloy. Likewise, the Hf concentrations are similar in the pit and in the alloy. Calcium concentrations in the pit were measured at a level less than 0.3%. These measurements indicate that Al is preferentially oxidized to a slightly greater extent than is Ti, causing some Ti to diffuse away from the growing pit. The slight Hf concentration gradient towards the pit could indicate the preferential oxidation of Hf although the low concentration measurements make this interpretation questionable

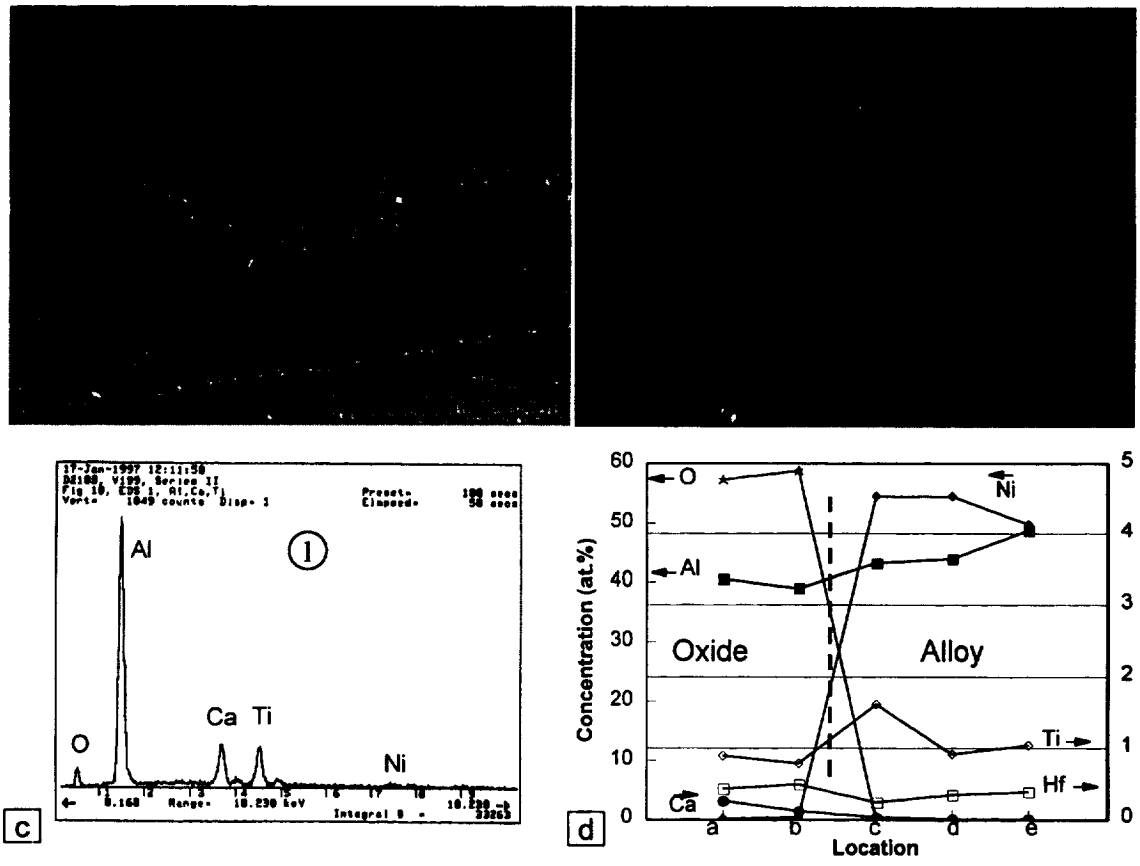

Figure 3. SEM micrographs showing possible pit initiation sites (a,b), EDS of the oxide in the pit (c) and concentrations in and below a broad, shallow pit (d).

As the corrosion pits grow, islands of the more-noble Ni were incorporated into the corrosion product. This stage of attack was considered "intermediate" between the initiation stage with the small pits and the rampant attack discussed below. An SEM micrograph of a region of intermediate attack is shown in Fig 4. Each region of intermediate attack contained islands of relatively pure Ni, either metallic or oxidized. A band of bright HfO_2 particles is again evident below the pit. Ca was detected in these larger pits, but not uniformly as in the smaller pits. No γ' phase was observed around any of the small pits.

Figure 4. SEM micrograph showing pit in intermediate attack stage. Lighter regions in pit are Ni or NiO. Bright particle in pit at 11 o'clock is HfC.

A rampant attack stage was identified at the corners of the sample, as shown in Fig 5. This accelerated attack was characterized by the rapid inward penetration of Al_2O_3 "fingers" which trapped large amounts of Al-depleted Ni within the scale. Often these Ni islands had been oxidized to NiO in the outer portion (nearer the oxide/gas interface) of the attacked region. At the corrosion front, near the ends of the Al_2O_3 fingers, the γ' phase was identified below a band of low-Al β (Fig 5b).

It is not clear what conditions lead to pit initiation. Obviously, the protective Al_2O_3 scale must be breached or inhibited from forming. The protective scale could have been partially or locally dissolved (fluxed) by sulfate deposits, or cracked and damaged by thermal cycling. Ca, and to a lesser extent, Mg were observed throughout the initiating pits and could induce the hot corrosion process. However, the near-absence of S and Na, both active elements in many hot corrosion processes, was surprising. The role which the HfO_2 stringers or the TiO_2 in the scale might play in allowing a molten sulfate to penetrate the scale is also uncertain. Additional testing for shorter times might reveal the conditions promoting pit initiation.

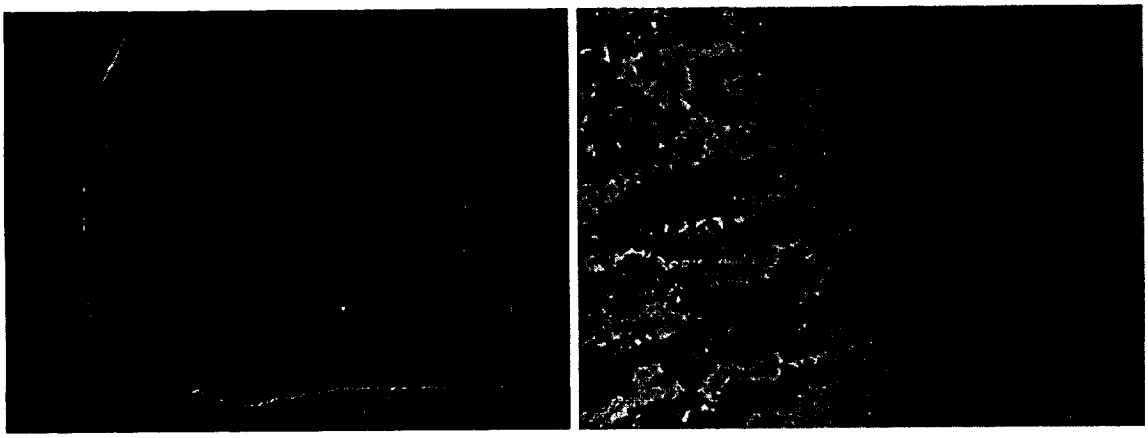

Figure 5. SEM micrograph of sample corner showing rampant stage of attack.

In summary, hot corrosion testing produced random mounds on the sample ends and curved surface of the sample. Areas between mounds showed a relatively smooth but duplex α-Al_2O_3 scale. The inner region of this scale contained HfO_2 particles and Ti was also detected

whereas the outer region appeared uniform without detectable Ti or Hf. Some TiO_2 was typically detected in the alumina scale. Cross-sectional microscopy indicates that the corrosion attack initiates with pits. The pits are primarily Al_2O_3 with small concentrations of HfO_2 and TiO_2. The oxide-filled pits rapidly grow inward and eventually encapsulate small regions of Ni. A rampant attack stage was characterized by an accelerated inward penetration of Al_2O_3 fingers which trapped large amounts of Ni within the scale. Only in this stage was the γ' phase detected.

REFERENCES

1. R. Darolia, JOM, 43, p. 43, 1991.

2. D.B. Miracle, Acta. Metall. Mater., **41**, 649, 1993.

3. W.S. Walston, R.D. Field, J.R. Dobbs, D.F. Lahrman and R. Darolia, "Microstructure and High-Temperature Strength of NiAl Alloys," in *Structural Intermetallics*, R. Darolia, J.J. Lewandowski, C.T. Liu, P.I. Martin, D.B. Miracle and M.V. Nathal, editors, TMS, Warrendale, 1993, p. 523-532.

4. J. Stringer, J. De Physique IV, **3**, 43, 1993

5. F.S. Pettit and C.S. Giggins, "Hot Corrosion," in *Superalloys II*, C.T. Sims, N.S. Stoloff and W.C. Hagel, editors, John Wiley and Sons, New York, 1987, p. 327-358.

6. M. Kaufman, Trans ASM, **62**, 590, 1969.

7. G. Romeo and D.W. McKee, J. Electrochem. Soc., **122**, 188, 1975.

8. R.L McCarron, N.R. Lindblad, and D. Chatterji, Corrosion, **2**, 476, 1976.

9. D.L. Ellis, "Hot Corrosion of the B2 Nickel Aluminides," NASA CR191082, March 1993.

10. J.A. Nesbitt, C.A. Barrett and P.O. Dickerson, NASA TM 107346, 1996.

11. J.A. Nesbitt, "Hot Corrosion of Single-Crystal NiAl-X Alloys," NASA TM 113128, 1998.

12. G.C. Rybicki and J.L. Smialek, Ox. Met., **31**, 275, 1989.

13. B.A. Pint, M. Treska and L.W. Hobbs, Ox. Met., **47**, 1, 1996.

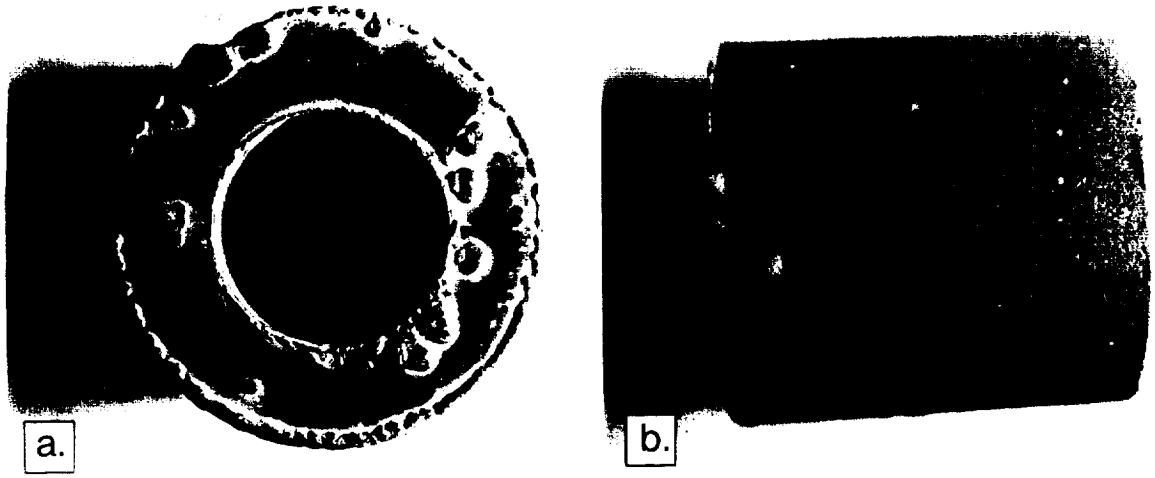

Figure 1. Macrophotos of one end and the curved surface after 300 hrs of testing.

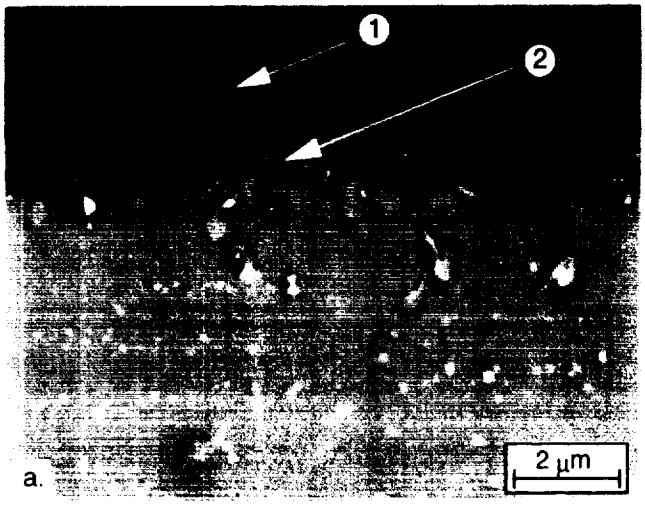

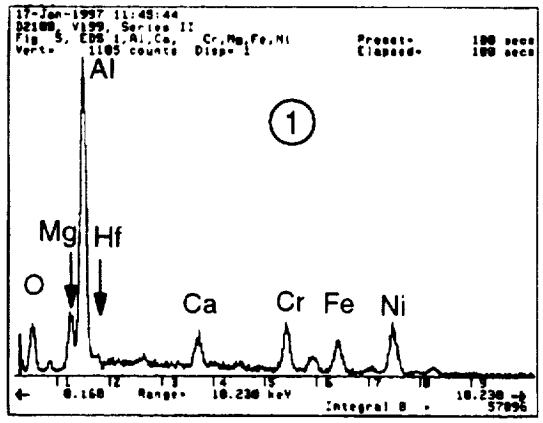

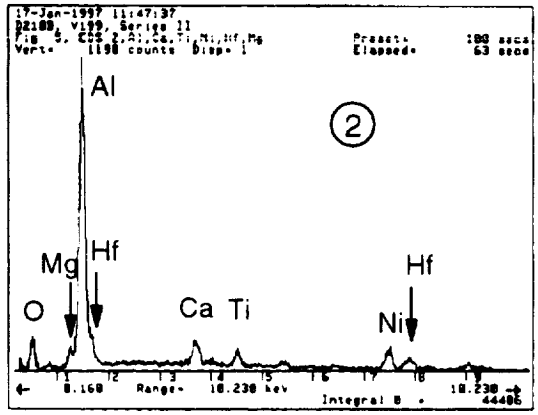

Figure 2. SEM cross-sectional microstructure of smooth scale. EDS of the outer region of the scale is shown in b. and of the inner region in c. Bright particles in inner region and in alloy are probably HfO_2.

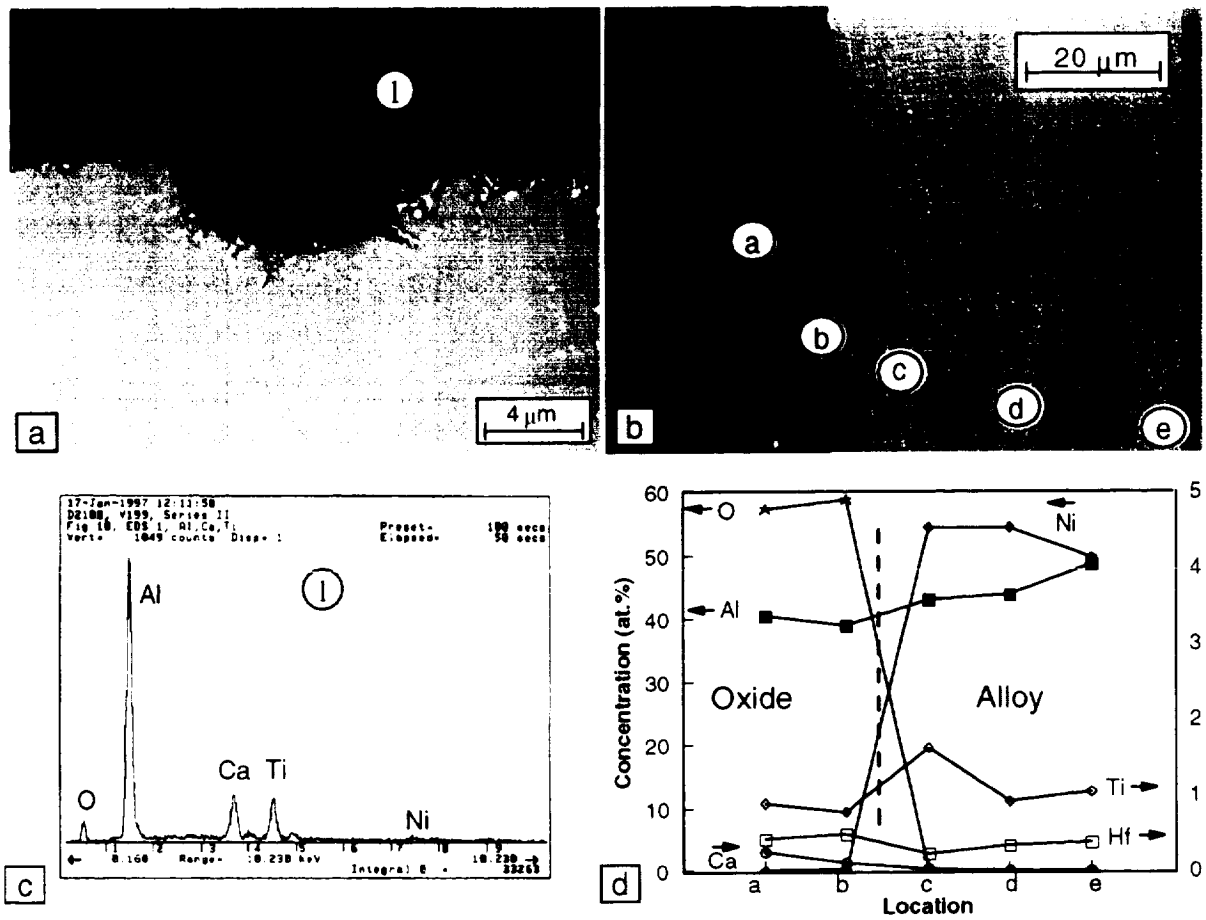

Figure 3. SEM micrographs showing possible pit initiation sites (a,b), EDS of the oxide in the pit (c) and concentrations in and below a broad, shallow pit (d).

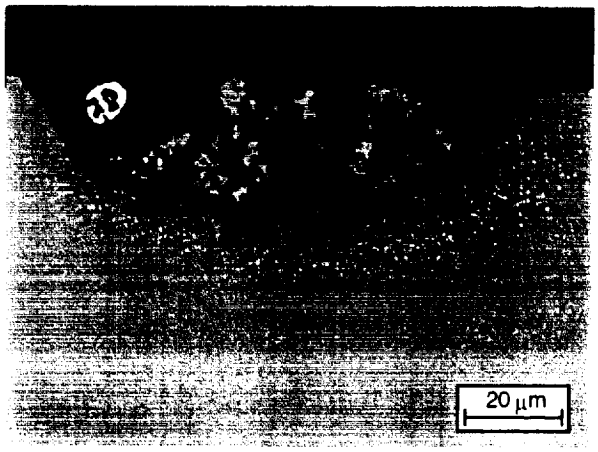

Figure 4. SEM micrograph showing pit in intermediate attack stage. Lighter regions in pit are Ni or NiO. Bright particle in pit at 11 o'clock is HfC.

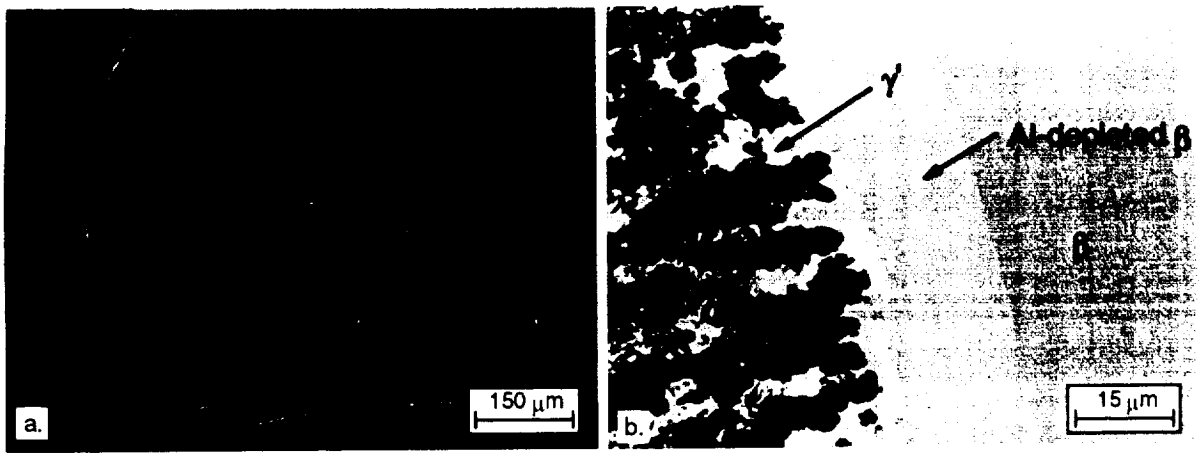

Figure 5. SEM micrograph of sample corner showing rampant stage of attack.